Author(s): Liang, Zhenhu; Ren, Ye; Yan, Jiaqing; Li, Duan; Voss, Logan J.; Sleigh, Jamie W.; Li, Xiaoli

Title: A comparison of different synchronization measures in electroencephalogram during propofol anesthesia

Year: 2016

Version: Accepted version (Final draft)

Please cite the original version:

Liang, Z., Ren, Y., Yan, J., Li, D., Voss, L. J., Sleigh, J. W., & Li, X. (2016). A comparison of different synchronization measures in electroencephalogram during propofol anesthesia. Journal of Clinical Monitoring and Computing, 30(4), 451-466. https://doi.org/10.1007/s10877-015-9738-z

A comparison of different synchronization measures in electroencephalogram during propofol anesthesia

Authors: Zhenhu Liang[1,2#], Ye Ren[1#], Jiaqing Yan[1], Duan Li[3], Logan J. Voss[4], Jamie W. Sleigh[4], Xiaoli Li[1,2*]

Affiliations:

[1] Institute of Electric Engineering, Yanshan University, Qinhuangdao 066004, China

[2] Key Laboratory of Industrial Computer Control Engineering of Hebei Province, Yanshan University, Qinhuangdao 066004, China

[3] Institute of Information Science and Engineering, Yanshan University, Qinhuangdao 066004, China

[4] Department of Anaesthesia, Waikato Hospital, Hamilton, New Zealand

[#] These authors equally contributed to this work.

* Correspondence to:

Prof. Xiaoli Li

Email: xlli@ysu.edu.cn

Abstract

Background: Electroencephalogram (EEG) synchronization is becoming an essential tool to describe neurophysiological mechanisms of communication between brain regions under general anesthesia. Different synchronization measures have their own properties to reflect the changes of EEG activities during different anesthetic states. However, the performance characteristics and the relations of different synchronization measures in evaluating synchronization changes during propofol-induced anesthesia are not fully elucidated.

Methods: Two-channel EEG data from seven volunteers who had undergone a brief standardized propofol anesthesia were then adopted to calculate eight synchronization indexes. We computed the prediction probability (P_K) of synchronization indexes with Bispectral Index (BIS) and propofol effect-site concentration (C_{eff}) to quantify the ability of the indexes to predict BIS and C_{eff}. Also, box plots and coefficient of variation (CV) were used to reflect the different synchronization changes and their robustness to noise in awake, unconscious and recovery states, and the Pearson correlation coefficient (R) was used for assessing the relationship among synchronization measures, BIS and C_{eff}.

Results: Permutation cross mutual information (PCMI) and determinism (DET) could predict BIS and follow C_{eff} better than nonlinear interdependence (NI), mutual information based on kernel estimation (KerMI) and cross correlation (COR). Wavelet transform coherence (WTC) in α and β frequency bands followed BIS and C_{eff} better than that in other frequency bands. There was a significant decrease in unconscious state and a significant increase in recovery state for PCMI and NI, while the trends were opposite for KerMI, DET and WTC. Phase synchronization based on phase locking value (PS_PLV) in δ, θ, α and γ1 frequency bands dropped significantly in unconscious state, whereas it had no significant synchronization in recovery state. Moreover, PCMI, NI, DET correlated closely with each other and they had a better robustness to noise and higher correlation with BIS and C_{eff} than other synchronization indexes.

Conclusions: Propofol caused EEG synchronization changes during the anesthetic period. Different synchronization measures had individual properties in evaluating synchronization changes in differ-

ent anesthetic states, which might be related to various forms of neural activities and neurophysiological mechanisms under general anesthesia.

1. Introduction

Understanding the neurophysiological mechanisms of anesthetic drug effect is an important issue for neuroscientists, anesthetists, as well as drug researchers [1]. Cognitive binding is thought to be a fundamental mechanism in human consciousness, and a number of recent studies suggest that loss of consciousness (LoC) during general anesthesia is associated with breakdown of long-distance cortical connectivity across multiple brain regions [2-5], especially in the frontal-parietal cortices [5]. Numerous measures, derived from different signal processing methods and statistics, have been proposed for quantifying neuro-synchronization [6-9] and some of the synchronization measures were used to interpret the mechanism of neural synchronization for general anesthesia. However, the performances of these synchronization measures for evaluating brain information integration or connectivity are not fully understand.

Cross correlation is based on the relationship of the magnitude of the electroencephalogram (EEG) signal between two regions, which is defined in the time domain. Lagged cross correlation was used to evaluate the interregional relationships of the blood-oxygen-level dependent signals of depressed people and natural sleep [10, 11]. However, few studies adopted the lagged cross correlation in the monitoring of anesthetic states. Coherence is a time-frequency domain method and it can evaluate the relationship of time series from different brain regions at different frequency bands. Many studies used some methods based on coherence in the coupling analysis during anesthesia. Li et al. combined the magnitude square coherence with S-estimator to analyzed the synchronization during sevoflurane anesthesia in sheep and they found that the synchronization increased from the waking to the burst-suppression states and decreased during recovery in the α and β frequency bands [12]. Hayashi et al. analyzed the bicoherence of frontal and occipital EEGs before and after induction of sevoflurane anesthesia and they found that there were delta and alpha power shift between frontal and occipital EEG with increasing sevoflurane concentration [13].

Phase synchronization analysis is a classical neuronal oscillation analysis method that is independent of the amplitude of the signal. It was sensitive to nonlinear coupling and it was a promising tool for quantifying coupling in multi-channel electroencephalogram or magnetoencephalogram (MEG) re-

cordings [14-16]. Koskinen et al. used the Hilbert transform based phase synchronization indices to investigate the phase coupling during propofol anesthetic induction and recovery periods and they found that the sub-delta band decreased during the induction and increased during the recovery, while the directions were reversed in the alpha band [17]. Nicolaou et al. analyzed how anesthesia affected widespread patterns of phase synchrony and they found anesthesia caused different phase synchronization changes in different frequency bands [18].

Mutual information is an information theory method and it has been widely applied in EEG analysis as a way of estimating information integration between different EEG channels or brain regions for mechanism analysis and neurological disease diagnosis, such as epilepsy seizure, Alzheimer's disease and autism [19-21]. We applied kernel density estimation and permutation entropy to quantify the mutual information. Kernel density estimation which was suggested by Moon et al. [22] was found to be superior to the histogram-based mutual information. However, there is no research using kernel density-based mutual information to evaluate the depth of anesthesia (DoA). On the contrary, permutation mutual information has been proved to be a promising method to tracking EEG dynamics during sevoflurane, isoflurane and remifentanil anesthesia [23, 24].

Nonlinear interdependence is a measure of generalized synchronization in nonlinear systems, which evaluates the interdependency according to the distance of delay vectors of two time series. It was most applied for evaluating the EEG functional connectivity, seizure prediction of epilepsy patients in different brain regions [25, 26]. However, few studies used the NI to characterize the EEG interdependence during anesthesia.

DET in the recurrence quantification analysis is based on the reconstruction of the phase space of the signals. High value of DET means strong synchronization of two time series, and vice versa. Recurrence quantification analysis has been applied to the monitoring of the depth of anesthesia and this technique had been proved that it could separates consciousness from unconsciousness during sevoflurane and propofol anesthesia [27]. Shalbaf et al. proposed the order patterns cross recurrence analysis to assess synchronization changes during propofol anesthesia [28].

Different measures for measuring synchronization rely on certain characteristic features of the dynamical system under investigation. However, the underlying dynamic properties of the synchronization measures applied to the EEG data in different anesthetic states are not completely known. We concentrated on the synchronization changes of two-channel EEG from prefrontal and primary motor cortices during propofol-induced anesthesia. We studied and compared a range of different synchronization measures: cross correlation (COR); magnitude squared coherence based on Fourier transform (FTC) and coherence based on wavelet transform (WTC); phase synchronization (PS) based on phase locking value, Shannon entropy and conditional probability; mutual information (MI) based on kernel density estimation and permutation; nonlinear interdependence (NI) and determinism (DET) in the recurrence quantification analysis (RQA). Using different synchronization measures, we aim to the describe their individual properties during the whole period of anesthesia, evaluate performance of distinguishing awake, unconscious and recovery states, find the effective measures for evaluating of clinical anesthetic depth, and help us to understand the underlying neurophysiological mechanisms of anesthesia.

This paper is organized as follows. Section 2 describes each synchronization measure and Section 3 gives the statistical analysis methods. In Section 4, the details of EEG recording, preprocessing and the results of the application of the synchronization measures to the real EEG are presented. Finally, the discussion and conclusion are given in Section 5. The parameter selection of some synchronization measures were discussed in Appendix.

2. Synchronization measures

2.1 Cross correlation

The cross correlation is one of the most well-known measures for evaluating the linear coupling relationship between two time series. Given two time series $x(t)$ and $y(t)$ ($t=1,2,\cdots,N$), the cross-correlation function [10, 29] is defined as

$$COR(\tau) = \frac{\text{cov}(x(t+\tau), y(t))}{\sqrt{\text{var}(x(t+\tau))\,\text{var}(y(t))}} \tag{1}$$

where $COR(\tau) = COR(-\tau)$ and it is restricted to the [-1,1] interval. τ is the time lag between two time series. When COR is positive, it implies that the two time series have strong synchronization relationship. By contrast, the negative COR represents that the synchronization of two time series is weak. $\tau=0$ corresponds to zero-order correlation and $COR(0)$ is used as the synchronization index in our study.

2.2 Coherence

Coherence is a frequency domain based method which measures the linear correlations of two time series [30]. In this study, we considered two coherence calculation methods: magnitude squared coherence based on Fourier transform and coherence based on wavelet transform.

Given two time series $x(t)$ and $y(t)$ ($t=1,2,\cdots,N$), the magnitude squared coherence is defined as a function of the power spectral densities $P_{xx}(f)$ and $P_{yy}(f)$, and the cross power spectral density $P_{xy}(f)$

$$C_{xy}(f) = \frac{|P_{xy}(f)|^2}{P_{xx}(f)P_{yy}(f)} \tag{2}$$

$C_{xy}(f)$ is a function of frequency with values between 0 and 1, and $P_{xy}(f) = X(f) \cdot Y^*(f)$ where $X(f)$ and $Y(f)$ are the Fourier transforms of $x(t)$ and $y(t)$ and * denotes the complex conjugate.

The wavelet-based coherence function is defined at time t and frequency f

$$C_{xy}^w(t,f) = \frac{\left|S_{xy}(t,f)\right|}{[S_{xx}(t,f)S_{yy}(t,f)]^{1/2}}$$ (3)

where $S_{xy}(t,f)$ is the wavelet cross-spectrum between $x(t)$ and $y(t)$,

$$S_{xy}(t,f) = \int_{t-\delta/2}^{t+\delta/2} W_x(\tau,f) \cdot W_y^*(\tau,f) d\tau$$ (4)

where $*$ denotes the complex conjugate and δ is a scalar that depends on frequency. $W_x(\tau,f)$ and $W_y(\tau,f)$ are the wavelet transform of $x(t)$ and $y(t)$, and Morlet wavelet transform(MWT) is employed in this study,

$$W_x(\tau,f) = \frac{1}{\sqrt{f}} \int_{-\infty}^{+\infty} x(t)\psi^*\left(\frac{t-\tau}{f}\right) dt$$ (5)

where $\psi(t) = \pi^{-\frac{1}{4}} e^{iw_0 t} e^{-\frac{1}{2t^2}}$, w_0 is the wavelet central angle frequency which is an optional value to adjust the time-frequency resolution, often $w_0 \geq 6$. The details are described in [31].

The *WTC* index is used to evaluate synchronization in our study and the *WTC* index at the frequency band $[f_L, f_H]$ is defined as

$$WTC(t) = \frac{1}{N_w} \sum_{f=f_L}^{f_H} C_{xy}^w(t,f)$$ (6)

where N_w is the number of summands in the summation, *WTC* ranges from 0 to 1 [12].

The *WTC* index is calculated across five frequency bands: δ (1-4 Hz), θ (4-8 Hz), α (8-13 Hz), β (13-30 Hz) and γ1 (30-40 Hz) in our study.

2.3 Phase synchronization

Phase synchronization (PS) analysis has been independently proposed by Lachaux et al. [32], Mormann et al. [33] and is applied later by Allefeld and Kurths [34, 35]. This approach is based on the

concept of synchronization of chaotic oscillators studied by Rosenblum et al [36]. There are various estimation methods of phase synchronization. Instantaneous phase estimation and phase coupling quantification are the two fundamental steps in phase synchronization evaluation.

Li et al employed the windowed harmonic wavelet transform (WHWT) to extract the instantaneous phase of brain signals, and shows that WHWT performs better than traditional methods, such as the Hilbert transform (HT) [37]. So we chose WHWT to calculate the instantaneous phase in this study. The algorithm is described as follows:

Given two time series $x(t)$ and $y(t)$ ($t = 1,2,\cdots,N$) and their Fourier transforms are $X(f)$ and $Y(f)$ which are used to achieve the corresponding expressions in the frequency domain. Then, multiplying $X(f)$ by the conjugate of the windowed harmonic wavelet of $Y(f)$ and denoted as $A(f) = X(f)Y_w^*(f)$. Taking the inverse Fourier transform of $A(f)$ to obtain the signal with WHWT, which is presented by [38]

$$a(t) = u(t) + iH[u(t)] = u(t) + \frac{i}{\pi}\int_{-\infty}^{\infty}\frac{u(\tau)}{t-\tau}d\tau = S(t)e^{i\varphi(t)} \tag{7}$$

where $H[\cdot]$ stands for Hilbert transform. The magnitude of $a(t)$ is represented as $S(t) = \sqrt{(u(t))^2 + (H[u(t)])^2}$ and the instantaneous phase of $a(t)$ is

$$\varphi(t) = \tan^{-1}\left(\frac{H[(u(t)]}{u(t)}\right) = \tan^{-1}\left(\frac{imag[a(t)]}{real[a(t)]}\right) \tag{8}$$

The instantaneous phase $\varphi_x(t)$ and $\varphi_y(t)$ can be achieved through the WHWT and the phase difference is $\Delta\varphi_{xy}(t) = \varphi_x(t) - \varphi_y(t)$.

There are three PS measures considered in this study. The first PS measure uses the phase locking value (PLV) [39], denoted as PS_{PLV}. The calculation is based on a time window with a specified length L,

$$PS_{PLV} = \frac{1}{L}\left|\sum_{t=1}^{L}e^{i\Delta\varphi_{xy}(t)}\right| \tag{9}$$

where PS$_{PLV}$ is bound between 0 and 1.

The second PS measure is based on Shannon entropy (PS$_{SE}$) of the distribution of $\Delta\varphi_{xy}(t)$ [40].

The $\psi = \Delta\varphi_{xy}(t)\bmod 2\pi$ is divided into M bins and p_k is the probability that ψ is in the bin k.

Then this PS measure is defined as

$$PS_{SE} = \frac{S_{\max} - S}{S_{\max}} \tag{10}$$

where $S = -\sum_{k=1}^{M} p_k \ln p_k$ and $S_{\max} = \ln M$ .It ranges from 0 for a uniform distribution of $\Delta\varphi_{xy}(t)$,to

1 if the distribution is a delta function. The optimum number of M is found as $e^{0.626+0.4\ln(L-1)}$ [41],

where L is the number of data points in a time window.

The third PS measure is based on conditional probability (PS$_{CP}$) [40] and it is described as follows:

Dividing the interval $[0,2\pi]$ into K ($k = 1,2,\cdots,K$) bins and binning the phase of time series $x(t)$

into K phase bins. The value of $\varphi_x(t)\bmod 2\pi$ falling into the k-th bin is denoted as $\theta_k(t)$ and the

number of points within the bin are denoted as M_k . Then, for all the time points when

$\varphi_x(t)\bmod 2\pi$ belongs to the k-th bin, we compute the corresponding phase value $\varphi_y(t)\bmod 2\pi$ of

time series $y(t)$ and denote them as $\eta_k(t)$. The PS index is denoted as

$$PS_{CP} = \frac{1}{K}\sum_{k=1}^{K}|\Lambda_k| \tag{11}$$

where $\Lambda_k = \frac{1}{M_k}\sum_t e^{i\eta_k(t)}$.

Each PS index is calculated across the frequency bands δ, θ, α, β and γ1. We divide the EEG data into a series of time epochs and the discussion of PS indexes at different epoch lengths T_e is shown in **Appendix A(1)**.

2.4 Mutual information based on kernel estimation (KerMI)

The mutual information evaluates the interdependence between variables and is widely used to analyze nonlinear systems. Given two discrete random variables X and Y, $p_X(x_i)$ $(i=1,2,\cdots,b_X)$ is the marginal probability of the event $X=x_i$, $p_Y(y_j)$ $(j=1,2,\cdots,b_Y)$ is the marginal probability of the event $Y=y_i$ and $p_{XY}(x_i,y_j)$ is the joint probability of the event $X=x_i, Y=y_j$. Then the mutual information between X and Y is defined as

$$I(X,Y)=\sum_{i,j}p_{XY}(x_i,y_j)\log\frac{p_{XY}(x_i,y_j)}{p_X(x_i)p_Y(y_j)} \tag{12}$$

As for the discrete random variables $X=x(t)$ and $Y=y(t)$ $(t=1,2,\cdots,N)$, the most straightforward approach for estimating probabilities is partitioning $x(t)$ and $y(t)$ into K ($k=1,2,\cdots,K$) bins of finite size, and counting the numbers of points falling into the each bins. The number of points within the bin are denoted as $M_X(k)$, $M_Y(k)$ and $M_{XY}(k)$. Then, the marginal and joint probabilities can be denoted as $p_X(k)=\dfrac{M_X(k)}{N}$, $p_Y(k)=\dfrac{M_Y(k)}{N}$ and $p_{XY}(k)=\dfrac{M_{XY}(k)}{N}$ respectively.

Kernel techniques are an attractive alternative to binning a distribution which is discussed thoroughly in [42]. Rather than simply counting the points, we can determine the distance-dependent weight of each point by using kernel function. Then, the marginal probability density and joint probability density which are estimated by the Gaussian kernel estimator [43] can be denoted as [44, 45],

$$p_X\big(x(t)\big)=\frac{1}{N}\frac{1}{\sqrt{2\pi h^2}}\sum_{\tilde{t}=1}^{N}e^{-\frac{1}{2h^2}(x(t)-x(\tilde{t}))^2}, p_Y\big(y(t)\big)=\frac{1}{N}\frac{1}{\sqrt{2\pi h^2}}\sum_{\tilde{t}=1}^{N}e^{-\frac{1}{2h^2}(y(t)-y(\tilde{t}))^2} \tag{13}$$

$$p_{XY}\big(x(t),y(t)\big)=\frac{1}{N}\frac{1}{2\pi h^2}\sum_{\tilde{t}=1}^{N}e^{-\frac{1}{2h^2}((x(t)-x(\tilde{t}))^2+(y(t)-y(\tilde{t}))^2)} \tag{14}$$

where parameter h is called window width of the kernels.

Last, we obtain the mutual information based on kernel estimation,

$$KerMI=\sum_{t=1}^{N}p_{XY}\big(x(t),y(t)\big)\log\left[\frac{p_{XY}(x(t),y(t))}{p_X\big(x(t)\big)p_Y\big(y(t)\big)}\right] \tag{15}$$

The approximately optimal window width h is given by $h_{opt} \approx \sigma \left(\dfrac{4}{d+2} \right)^{1/(d+4)} N^{-1/(d+4)}$ with $d=2$ being the dimension of Gaussian kernel estimation and σ the average marginal SD [42].

2.5 Permutation cross mutual information (PCMI)

Order pattern analysis is an important method for studying nonlinear dynamical time series [46]. Calculation of the probability distribution of the order patterns is the core of PCMI calculation. Given the time series $X = x(t)$ and $Y = y(t)$ ($t = 1,2,\cdots,N$), we can obtain the embedding vector

$$\mathbf{x}_i = [x(i), x(i+\tau),\cdots, x(i+(m-1)\tau)] \qquad \text{and} \qquad \mathbf{y}_i = [y(i), y(i+\tau),\cdots, y(i+(m-1)\tau)]$$

($i = 1,2,\cdots,N-(m-1)\tau$) with the embedding dimension m and time lag τ. Then, sorting the elements of vectors $\mathbf{x}_i$ and $\mathbf{y}_i$ in ascending order respectively and there are $m!$ possible order patterns in each vectors, which is also called permutations. Next, counting the number of each order pattern of all vectors $C_X(k)(k=1,2,\cdots,m!)$ and $C_Y(l)(l=1,2,\cdots,m!)$, and we can obtain the probability of each permutation $p_X(k) = \dfrac{C_X(k)}{N-(m-1)\tau}$ and $p_Y(l) = \dfrac{C_Y(l)}{N-(m-1)\tau}$.

Based on Shannon information theory, the permutation entropy (PE) of X and Y is

$$PE_X = -\sum_{k=1}^{m!} p_X(k) \ln p_X(k) \, , \, PE_Y = -\sum_{l=1}^{m!} p_Y(l) \ln p_Y(l) \tag{16}$$

The joint permutation entropy of X and Y is

$$PE_{XY} = -\sum_{k=1}^{m!} \sum_{l=1}^{m!} p_{XY}(k,l) \ln p_{XY}(k,l) \tag{17}$$

where $p_{XY}(k,l)$ is the joint probability of permutation of vectors $\mathbf{x}_i$ and $\mathbf{y}_i$.

Then, the *PCMI* of X and Y is defined as

$$PCMI = PE_X + PE_Y - PE_{XY} \tag{18}$$

Previous study found that the parameter selection $m=6$ and $\tau=1$ when the sampling rate of data is 100

Hz resulted in the best *PCMI* performance in distinguish different anesthetic state [47]. Therefore, we used *m*=6 and τ=1 for the calculation of *PCMI* index in this study.

2.6 Nonlinear interdependence

Nonlinear interdependence is an important nonlinear synchronization measure in neural systems [48-51]. The details of the algorithm are described as follows:

Given the time series $X = x(t)$ and $Y = y(t)$ ($t = 1,2,\cdots,N$), we can reconstruct delay vectors the embedding vector $\mathbf{x}_i = [x(i), x(i+\tau),\cdots, x(i+(m-1)\tau)]$ and $\mathbf{y}_i = [y(i), y(i+\tau),\cdots, y(i+(m-1)\tau)]$ ($i = 1,2,\cdots,Q$, $Q = N - (m-1)\tau$) with the embedding dimension *m* and time lag τ. We first denote $r_{i,j}$ and $s_{i,j}$, $j = 1,\cdots,k$ as the time indices of the *k* nearest neighbors of $\mathbf{x}_i$ and $\mathbf{y}_i$, respectively. For each $\mathbf{x}_i$, the mean squared Euclidean distance to its *k* neighbors is defined as

$$R(\mathbf{x}_i) = \frac{1}{k}\sum_{j=1}^{k}(\mathbf{x}_i - \mathbf{x}_{r_{i,j}})^2 \tag{19}$$

The *y*-conditioned mean squared Euclidean distance is defined by replacing the nearest neighbors by the equal time partners of the closest neighbors of $\mathbf{y}_i$

$$R(\mathbf{x}_i|\mathbf{y}_i) = \frac{1}{k}\sum_{j=1}^{k}(\mathbf{x}_i - \mathbf{x}_{s_{i,j}})^2 \tag{20}$$

We can define the nonlinear interdependence [52]

$$NI(X|Y) = \frac{1}{Q}\sum_{i=1}^{Q}\frac{R(\mathbf{x}_i)}{R(\mathbf{x}_i|\mathbf{y}_i)} \tag{21}$$

The $NI(X|Y)$ ranges from 0 if the two time series are independent $R(\mathbf{x}_i|\mathbf{y}_i) \approx R(X) >> R(\mathbf{x}_i)$, to 1 if they are highly correlated $R(\mathbf{x}_i|\mathbf{y}_i) \approx R(\mathbf{x}_i) << R(X)$, where $R(X) = 1/Q\sum_{i=1}^{Q}R(\mathbf{x}_i), k = Q-1$.

The selection of three parameters of *NI*: embedding dimension *m*, time lag τ and the number of nearest neighbors *k* is discussed in **Appendix A(2)**.

2.7 Cross recurrence analysis

The recurrence of states, meaning that states are arbitrarily close after some time, is a fundamental property of dynamical systems [53]. The cross recurrence plot (CRP) which is a bivariate extension of the recurrence plot (RP) is introduced to analyze the dependencies between two different systems [54, 55].

Considering two time series $x(t)$ and $y(t)$ ($t = 1, 2, \cdots, N$), we reconstruct the embedding vector

$$\mathbf{x}_k = [x(k), x(k+\tau), \cdots, x(k+(m-1)\tau)] \quad \text{and} \quad \mathbf{y}_k = [y(k), y(k+\tau), \cdots, y(k+(m-1)\tau)]$$

($k = 1, 2, \cdots, N - (m-1)\tau$) with the embedding dimension m and time lag τ. The cross recurrence matrix which is also called cross recurrence plot is defined by,

$$CR_{i,j} = \Theta(\varepsilon - \|\mathbf{x}_i - \mathbf{y}_j\|) \quad i, j = 1, 2, \cdots, Q \tag{22}$$

where ε is the threshold distance, $\Theta(\cdot)$ is the Heaviside function, $\|\cdot\|$ is the Euclidean norm and Q is the number of embedding vector.

The recurrence quantification analysis [56, 57] defined several measures based on diagonal oriented lines in RP, such as recurrence rate, determinism (DET), maximal length of diagonal structures, entropy and trend. The determinism is ratio of recurrence points forming diagonal structures (of at least length l_{min}) to all recurrence points in CRP. Long diagonal structures show similar phase space behavior of two time series, while stochastic time series cause short diagonals. In our study, we use *DET* to evaluate the synchronization of the two time series,

$$DET = \frac{\sum_{l=l_{min}}^{Q} lP(l)}{\sum_{l=1}^{Q} lP(l)} \tag{23}$$

where l is the length of the diagonal which parallels the main diagonal, $P(l)$ is the corresponding distribution probability. l_{min} is the threshold of diagonal length.

The selection of three parameters of *DET*: embedding dimension m, time lag τ and threshold of diagonal length l_{min} is discussed in **Appendix A(3)**.

3. Statistical analysis

The aim of this study is to evaluate the performance of different synchronization measures for tracking synchronization changes during anesthetic period and the ability of distinguish different anesthetic states. We used the prediction probability (P_K) [58, 59] to evaluate the ability of predicting BIS and propofol effect-site concentration (C_{eff}) (derived from pharmacokinetic/pharmacodynamic (PK/PD) modeling [60]) of all synchronization measures.

Given the BIS or C_{eff} value $S(k), k = 1,2,\cdots,N$ and the synchronization index $I(k), k = 1,2,\cdots,N$, we choose two data points $S(i)$ and $S(j)$ $(S(i) \neq S(j), i \neq j)$ randomly. Then, we compare the monotony of $I(i)$ and $I(j)$ with the monotony of $S(i)$ and $S(j)$. If $I(i) = I(j)$, $I(i)$ and $I(j)$ are considered as an x-only tie. If the monotony of $I(i)$ and $I(j)$ is same as the monotony of $S(i)$ and $S(j)$, $I(i)$ and $I(j)$ are considered as a concordance. Otherwise, they are considered as a discordance. We repeat the above steps for 500 times, then the P_K is defined as

$$P_K = \frac{P_c + P_{tx}/2}{P_c + P_d + P_{tx}} \tag{24}$$

where P_c, P_d, P_{tx} are the proportions that $I(i)$ and $I(j)$ are a concordance, discordance and an x-only tie respectively. P_K ranges from 0 to 1. P_K=1 means that the synchronization index predicts the BIS or C_{eff} correctly 100% of the time. P_K=0.5 means that the synchronization index correctly predicts that BIS or C_{eff} only 50% of the time. The P_K value is replaced by 1- P_K when there is a negative monotonic relationship between the synchronization indexes with BIS and C_{eff}.

Matlab Statistics Toolbox was applied for statistics. Kolmogorov-Smirnov test (*kstest.m*) was used to compare the P_K values of all synchronization measures to a standard normal distribution. We used the Friedman test (*friedman.m*) and Multiple comparison test (*multcompare.m*) to determine statistical significant difference among the P_K values of all synchronization indexes with BIS and C_{eff}. Box plot was adopted to evaluate the performance for distinguishing different anesthetic states of each synchronization index. Kolmogorov-Smirnov test was also used to compare the index values of syn-

chronization measures at awake, unconscious and recovery states of all subjects to a standard normal distribution. Kruskal-Wallis test (*kruskalwallis.m*) and Multiple comparison test were used to determine the significant difference of the index values between awake and unconscious states and between unconscious and recovery states. The coefficient of variation (CV) (the ratio of standard deviation (SD) to mean) was used to evaluate the index stability during propofol-induced anesthesia process [61]. Moreover, in order to gain the relation among different synchronization measures, Bispectral Index (BIS) and C_{eff}, we calculated the Pearson correlation coefficient R of all subjects.

4. Application to real EEG recordings and results

4.1 Subjects and EEG recordings

We studied the EEG data of seven human volunteers from previously published work [60]. With the permission of the Waikato Hospital Ethical Committee, the volunteers (American Society of Anesthesiologists physical status I or II) were recruited to undergo a brief propofol anesthetic and recovered in accordance with normal procedures of the Australian and New Zealand College of Anaesthesia (A.N.Z.C.A) guidelines. All subjects gave written informed consent after obtaining the permission of the hospital ethical committee. The silver-silver chloride scalp electrodes were placed at the position of Fp1-F7 and C3-T3 according to the 10-20 international system to produce bipolar signals (Fig. 1A). The ground electrode was placed at FpZ. The Aspect A-1000 EEG monitor (Aspect Medical Systems, Natick, MA, USA) was used to collected both the raw EEG signal (The sampling frequency is 256 Hz) and the BIS (The sampling frequency is 0.2 Hz).

The experimental sequence diagram is shown in Fig. 1B. The propofol intravenous infusion was 150ml/h (1500mg/h) in an antecubital vein via a syringe driver pump initially, and the BIS and raw EEG data were recorded when the infusion started. Then, a verbal list of dissimilar objects was read to the subject at 30-second intervals who held a syringe filled with water between forefinger and thumb. When the syringe dropped (LoC time), the infusion and the read of the list of dissimilar stopped, and the time was recorded as "syringe-drop time". The subject was then allowed to awake and given the play of a pre-recorded tape of random numbers and some verbal commands such as "move your right foot". The verbal commands lasted 5 seconds and they were at 10-second intervals. We recorded the time as "command time" as soon as the subject responded the verbal command correctly (recovery of consciousness (RoC) time). The subject were questioned as to the first number that they could recall and the last object that they could remember during propofol induction, and these two time points were recorded as "number time" and "object time" respectively. The study was terminated about 60 seconds after LoC time. The study four recorded times of all subjects are shown in Table 1.

"Fig. 1"

"Table 1"

4.2 EEG preprocessing

Generally, there are three main artifacts in EEG recordings: baseline drift, head movement noise and physiological noise (such as electrooculogram (EOG) and electromyogram (EMG)). For each source of noise we adopted a different artifact-rejection approach. Firstly, baseline drift and head movement noise are usually in the low frequency band (<0.5 Hz) and the function *eegfilt.m* in EEGLAB was used to reduce this noise [62]. Low-pass filter and the mains notch were set at 70 Hz and 50 Hz respectively. Secondly, raw EEG data exceeding an amplitude of 200 μV were removed as outlier points. Using statistical mean and standard deviation (SD) methods [63], amplitude values beyond the range mean$\pm$2SD were also considered as outliers. Then, EOG artifacts were reduced through a stationary wavelet transform based on an appropriate threshold [61]. Inverse filtering was used to identify transient events in the EEG, and was the method employed to detect and remove EMG and other high-amplitude transient artifacts [64, 65]. Finally, the EEG data were downsampled to 100 Hz by the function *resample.m* in Matlab.

In our study, in order to evaluate the synchronization during the whole experimental period, the EEG data were divided into a series of 10-second epochs, with an overlap of 75% (In particular, the data were divided into different length of time epoch for the calculation of PS indexes.). We used the EEG data in each epochs to calculate the synchronization indexes. Also, we chose three states from the whole period: awake state (the period before "Object time"), unconscious state (the period between LoC time and "Number time") and recovery state (the period after "command time") in order to evaluate the ability of different synchronization measures to distinguish different anesthetic states.

4.3 Results

We first analyzed the FTC and WTC of the two-channel EEG signals of all subjects to find a better coherence method to quantify the synchronization in frequency domain. The EEG recordings of two channels from one subject and their corresponding time-frequency spectrogram were shown in Fig. 2 A and Fig. 2B. The power in δ, α and β frequency bands increased with the increasing propofol ef-

fect-site concentration. Fig. 2C and Fig. 2D showed the FTC and WTC spectrums during the whole period. In terms of FTC spectrum, two-channel EEG signals were divided into a series of 10-second epochs with an overlap of 75%. The epochs were windowed using a Hamming window and FFT length was set to be 128. As can be seen from the figure, FTC spectrum could not reflect the changes of coherence during the whole period (Fig. 2C), while the WTC spectrum in the δ, α and β frequency bands increased obviously during unconscious state (Fig. 2D), which had the similar results as the spectrogram analysis. Therefore, we extracted the WTC index from WTC spectrum to quantify the synchronization during propofol-induced anesthesia period.

We then computed the synchronization indexes of all subjects during the whole anesthetic period. Fig. 3A was the preprocessed EEG signals of one subject from the left prefrontal and left primary motor cortex respectively. Fig. 3B and Fig. 3C were the corresponding BIS and C_{eff}. Fig. 3D showed the values of all synchronization indexes for the same subject. We computed three PS indexes at frequency bands δ, θ, α, β and γ1 and we found that the PS_{PLV} and PS_{CP} had similar results, which was consistent with previously reported results in [51], and the PS_{CP} will be not further reported. As can be seen from the Fig. 3D, the PCMI, NI, PS_{PLV} (δ, θ, α and γ1), PS_{SE} (δ, β) saw a decreasing trend with the increasing C_{eff} value, whereas KerMI, DET and WTC (δ, θ and α) showed an increasing trend which were consistent with the C_{eff}.

<div align="center">"Fig. 2"</div>

<div align="center">"Fig. 3"</div>

To quantify the ability of predicting BIS (P_{K_BIS}) and the relation with C_{eff} ($P_{K\_C_{eff}}$) of the synchronization measures, we calculated the P_K. The P_K values of each synchronization indexes with BIS and C_{eff} of all subjects and their corresponding box plots were shown in Fig. 4. The median (1st quartile (Q1), 3rd quartile (Q3)) of P_K values of all measures were displayed in Table 2. It can be seen from Fig. 4 and Table 2 that PCMI had the highest P_K value with BIS (P_{K_BIS}=0.855(0.775, 0.875)) and C_{eff} ($P_{K\_C_{eff}}$=0.794(0.703, 0.842)). DET ranked second with the value P_{K_BIS}=0.823(0.806, 0.869) and $P_{K\_C_{eff}}$=0.781(0.695, 0.816). These figures demonstrated that PCMI and DET could best

predict the BIS and follow the C_{eff}. The P_K values of NI, KerMI and COR were smaller than PCMI and DET. Kolmogorov-Smirnov test showed that the P_K values of each index were not normally distributed. The statistical significant difference among the synchronization indexes were marked at the top of Fig. 4A and B, using the notation *, ** and *** to indicate significant difference at $p<0.05$, $p<0.01$ and $p<0.001$ respectively (Friedman test and Multiple comparison test). As for PS_{PLV} and PS_{SE}, there was no significant difference among different frequency bands in tracking the BIS and C_{eff}. By contrast, WTC (α) predicted significantly better than WTC (γ1) with BIS, and WTC (α, β) predicted significantly better than WTC (γ1) with C_{eff} ($p<0.01$).

<center>"Fig. 4"</center>

<center>"Table 2"</center>

Furthermore, the ability to distinguish different anesthetic states of synchronization measures is essential for DoA monitoring. The synchronization indexes were computed at three anesthetic states (awake, unconscious and recovery) and the boxplots of the index values were shown in Fig. 5. The Kolmogorov-Smirnov test showed that the index value of each measure in each state were not normally distributed, so we adopted the Kruskal-Wallis test and Multiple comparison test to estimate the significant difference among between three states, using the notation *, ** and *** to indicate significant difference at $p<0.05$, $p<0.01$ and $p<0.001$ respectively. It can be seen from Fig. 5 that KerMI, PCMI, NI and DET could significantly distinguish awake and unconscious states as well as unconscious and recovery states ($p<0.001$), whereas COR could only distinguish awake and unconscious states ($p<0.001$). There was an increase in unconscious state and a decrease in recovery state for KerMI and DET, while the trends were opposite for PCMI and NI. In terms of PS_{PLV}, the phase synchronization dropped significantly in unconscious state for PS_{PLV} (δ, θ, α and γ1) and had no significant changes in recovery state, while PS_{PLV} (β) could not distinguish the three anesthetic states (Fig. 5F-J). PS_{SE} could only distinguish three states at θ and β frequency bands (Fig. 5K-O). As for WTC, there was a significant rise in unconscious state and a significant drop in recovery state for all frequency bands (Fig. 5P-T).

In addition, the stability of the index value during the anesthetic sates is important for the reliable DoA monitoring. We calculated the CV of all synchronization indexes of all subjects at awake, un-

conscious and recovery states and the CV values were shown in Table 3. As can be seen from Table. 3, PCMI had the low CV in awake state (CV=0.085), unconscious state (CV=0.146) and recovery state (CV=0.105). The CV of NI, PS_{PLV}, PS_{SE} and DET were lower than COR and KerMI, which were all smaller than WTC in awake and unconscious states. By contrast, the CV of COR, NI, PS_{PLV}, PS_{SE}, DET gained smaller values than KerMI and WTC in recovery state. These results illustrated that PCMI, NI, PS and DET had a better robustness to noise during the propofol-induced anesthesia.

"Fig. 5"

"Table 3"

To further evaluate the relationship among synchronization measures, BIS and C_{eff}, we calculated the correlation coefficients R among different synchronization measures, BIS and C_{eff} of all subjects and the averaged R over all subjects were shown in Fig. 6. KerMI, DET, WTC index curves and C_{eff} during the whole period were reversed when calculating the correlation coefficients. As can be seen from Fig. 6, PCMI had the highest correlation coefficient with BIS (R=0.846) and C_{eff} (R=0.739). DET ranked second with BIS (R=0.843) and C_{eff} (R=0.703) and NI also had a high value with BIS (R=0.729) and C_{eff} (R=0.638). As for PS and WTC, PS_{PLV} (δ) and WTC (α) correlated with BIS and C_{eff} higher than that of other frequency bands. In terms of the relation among different synchronization measures, PCMI correlated closely with DET (R=0.949) and NI (R=0.838). Strong relation was obtained between KerMI and WTC (δ) (R=0.833) and between NI and DET(R=0.798).

"Fig. 6"

5. Discussion and conclusions

Despite the emergence of many DoA monitoring over the last few years, the neurophysiological mechanisms by which anesthetic drugs caused loss of consciousness are still unknown [1]. Many studies suggest that long-range synchronization of neuronal populations is a fundamental principle of cortical processing and communication. Multi-channel EEG is more suited for understanding the mechanisms of anesthetic effect and it could provide a more robust measure of anesthetic depth for clinical application. In this study, we considered ten synchronization measures, including cross correlation, two coherence measures, three phase synchronization measures, two mutual information measures, nonlinear interdependence and cross recurrence analysis. We sought to identify synchronization changes of EEG between two brain regions during different anesthetic states and evaluate the performance in tracking anesthetic drug concentration and the ability of distinguishing different anesthetic states of the synchronization measures.

In our results, COR performed worse in correlating with BIS and C_{eff} and distinguishing the anesthetic states in this study. We compared the Fourier transform coherence and wavelet transform coherence. The results showed that the coherence based on wavelet transform could reflect the synchronization changes during anesthetic states (Fig. 2C and D) and we used the WTC index which was extracted from WTC spectrum to quantify the synchronization in our study. With increasing WTC in unconscious state and decreasing WTC in recovery state, propofol makes the neural oscillations more synchronous after loss of consciousness, which is consistent with previously reported results in the reference [12]. Furthermore, recent studies using bicoherence [13], global coherence [66] reflected different forms of EEG synchronization in various frequency bands at different brain region under general anesthesia. Therefore, the coherence based synchronization measures are essential and promising for evaluating the communication among brain regions and describe the mechanism of general anesthesia.

The instantaneous phase extraction was based on the WHWT which had been proved that it was better than Hilbert transform [37] and Phase locking and Shannon entropy were used to quantify the phase synchronization. The results showed that propofol caused a decrease phase synchronization in

δ, θ, α, β and γ1 frequency bands and PS_{PLV} performed better than PS_{SE} in distinguishing unconscious state from awake state. However, this founding is not consistent with other studies about phase synchronization changes during anesthesia, which may be due to the different EEG functional connectivity of subjects or patients under different anesthesia procedures.

PCMI is related to the probability distribution of permutation pattern. Our results of decreasing PCMI in unconscious state and increasing PCMI in recovery state revealed that propofol lead to the decrease of permutation pattern of EEG signals, which means that the EEG signal is more regular when anesthetized [67, 68]. Also, PCMI presented a better performance than other indexes in evaluating EEG synchronization changes during anesthesia. It has the highest P_K and R values with BIS and C_{eff} (Fig. 4), strong robustness to noise and it can significantly distinguish awake, unconscious and recovery states (Fig. 5).These results illustrated that PCMI is a meaningful measure for characterizing EEG dynamics during anesthesia. As for KerMI, Gaussian kernel was used to quantify the probability density of mutual information. Our results showed that KerMI increased with increasing depth of anesthesia, which had an opposite trend with PCMI. Maybe it is the regular EEG signals in unconscious state which have small difference between adjacent signals that makes the increasing KerMI in unconscious state.

As for NI, the significant drop of NI in unconscious state in our study demonstrates that propofol weaken the interdependence and lead to the disconnection of two brain regions, which has been previously reported that brain functional integration decreased during propofol-induced loss of consciousness [5, 69]. Also, NI had close relation with BIS and C_{eff} and the ability to distinguish different anesthetic states. Therefore, as a nonlinear synchronization index, NI is suit for detecting the changes of interdependence of EEG signal during anesthesia.

DET performed good in following the C_{eff} and had good robustness to noise. Increasing in unconscious states and decreasing in recovery state means that propofol causes the increase of synchronization, which is consistent with the result in the recent study [28]. Accordingly, DET can be effectively evaluate the EEG synchronization changes during anesthesia.

In conclusion, most synchronization measures can detect the EEG dynamics during anesthesia. Each measure has their properties and performance on evaluating synchronization changes because of their own calculating principles, which may reflect different mechanism of anesthesia. Although our experiment data are limited which means that more investigation of these synchronization measures should be conducted for describing the underlying dynamics of these measures, we still characterize the EEG dynamics during propofol-induced anesthesia using different synchronization measures.

Conflict of interest

None declared.

Acknowledgments

References

1. Lewis LD, Weiner VS, Mukamel EA, Donoghue JA, Eskandar EN, Madsen JR, Anderson WS, Hochberg LR, Cash SS, Brown EN. Rapid fragmentation of neuronal networks at the onset of propofol-induced unconsciousness. Proceedings of the National Academy of Sciences 2012, 109(49).E3377-E3386.

2. Voss L, Sleigh J. Monitoring consciousness: the current status of EEG-based depth of anaesthesia monitors. Best Practice & Research Clinical Anaesthesiology 2007, 21(3).313-325.

3. Nallasamy N, Tsao DY. Functional connectivity in the brain: effects of anesthesia. The Neuroscientist 2011, 17(1).94-106.

4. Lee U, Mashour GA, Kim S, Noh G-J, Choi B-M. Propofol induction reduces the capacity for neural information integration: implications for the mechanism of consciousness and general anesthesia. Consciousness and cognition 2009, 18(1).56-64.

5. Lee U, Kim S, Noh G-J, Choi B-M, Hwang E, Mashour GA. The directionality and functional organization of frontoparietal connectivity during consciousness and anesthesia in humans. Consciousness and cognition 2009, 18(4).1069-1078.

6. Pereda E, Quiroga RQ, Bhattacharya J. Nonlinear multivariate analysis of neurophysiological signals. Progress in neurobiology 2005, 77(1).1-37.

7. Breakspear M. "Dynamic" connectivity in neural systems. Neuroinformatics 2004, 2(2).205-224.

8. Kaminski M, Liang H. Causal influence: advances in neurosignal analysis. Critical Reviews™ in Biomedical Engineering 2005, 33(4).

9. Stam CJ. Nonlinear dynamical analysis of EEG and MEG: review of an emerging field. Clinical Neurophysiology 2005, 116(10).2266-2301.

10. Siegle GJ, Thompson W, Carter CS, Steinhauer SR, Thase ME. Increased amygdala and decreased dorsolateral prefrontal BOLD responses in unipolar depression: related and independent features. Biol Psychiatry 2007, 61(2).198-209.

11. He BJ, Snyder AZ, Zempel JM, Smyth MD, Raichle ME. Electrophysiological correlates of the brain's intrinsic large-scale functional architecture. Proc Natl Acad Sci U S A 2008, 105(41).16039-16044.

12. Li D, Voss LJ, Sleigh JW, Li X. Effects of volatile anesthetic agents on cerebral cortical synchronization in sheep. Anesthesiology 2013, 119(1).81-88.

13. Hayashi K, Mukai N, Sawa T. Simultaneous bicoherence analysis of occipital and frontal electroencephalograms in awake and anesthetized subjects. Clin Neurophysiol 2014, 125(1).194-201.

14. David O, Cosmelli D, Friston KJ. Evaluation of different measures of functional connectivity using a neural mass model. Neuroimage 2004, 21(2).659-673.

15. Engel AK, Fries P, Singer W. Dynamic predictions: oscillations and synchrony in top–down processing. Nature Reviews Neuroscience 2001, 2(10).704-716.

16. David O, Friston KJ. A neural mass model for meg/eeg:: coupling and neuronal dynamics. Neuroimage 2003, 20(3).1743-1755.

17. Koskinen M, Seppanen T, Tuukkanen J, Yli-Hankala A, Jantti V. Propofol anesthesia induces phase synchronization changes in EEG. Clin Neurophysiol 2001, 112(2).386-392.

18. Nicolaou N, Georgiou J. Spatial Analytic Phase Difference of EEG activity during anesthetic-induced unconsciousness. Clin Neurophysiol 2014, 125(10).2122-2131.

19. Abásolo D, Escudero J, Hornero R, Gómez C, Espino P. Approximate entropy and auto mutual information analysis of the electroencephalogram in Alzheimer's disease patients. Medical & biological engineering & computing 2008, 46(10).1019-1028.

20. Hall Jr CW, Sarkar A. Mutual information in natural position order of electroencephalogram is significantly increased at seizure onset. Medical & biological engineering & computing 2011, 49(2).133-141.

21. Langen M, Schnack HG, Nederveen H, Bos D, Lahuis BE, de Jonge MV, van Engeland H, Durston S. Changes in the developmental trajectories of striatum in autism. Biological psychiatry 2009, 66(4).327-333.

22. Moon Y-I, Rajagopalan B, Lall U. Estimation of mutual information using kernel density estimators. Physical Review E 1995, 52(3).2318.

23. Liang Z, Wang Y, Ouyang G, Voss LJ, Sleigh JW, Li X. Permutation auto-mutual information of electroencephalogram in anesthesia. J Neural Eng 2013, 10(2).026004.

24. Liang Z, Liang S, Wang Y, Ouyang G, Li X. Tracking the coupling of two electroencephalogram series in the isoflurane and remifentanil anesthesia. Clin Neurophysiol 2014.

25. Andrzejak RG, Schindler K, Rummel C. Nonrandomness, nonlinear dependence, and nonstationarity of electroencephalographic recordings from epilepsy patients. Phys Rev E Stat Nonlin Soft Matter Phys 2012, 86(4 Pt 2).046206.

26. Rabbi AF, Azinfar L, Fazel-Rezai R. Seizure prediction using adaptive neuro-fuzzy inference system. Conf Proc IEEE Eng Med Biol Soc 2013, 2013.2100-2103.

27. Becker K, Schneider G, Eder M, Ranft A, Kochs EF, Zieglgansberger W, Dodt HU. Anaesthesia monitoring by recurrence quantification analysis of EEG data. PLoS One 2010, 5(1).e8876.

28. Shalbaf R, Behnam H, Sleigh JW, Steyn-Ross DA, Steyn-Ross ML. Frontal-Temporal Synchronization of EEG Signals Quantified by Order Patterns Cross Recurrence Analysis During Propofol Anesthesia. IEEE Trans Neural Syst Rehabil Eng 2014.

29. Zhou D, Thompson WK, Siegle G. MATLAB toolbox for functional connectivity. Neuroimage 2009, 47(4).1590-1607.

30. Nunez PL. Electric fields of the brain: the neurophysics of EEG. Oxford University Press; 2006.

31. Li X, Yao X, Fox J, Jefferys JG. Interaction dynamics of neuronal oscillations analysed using wavelet transforms. Journal of neuroscience methods 2007, 160(1).178-185.

32. Lachaux JP, Rodriguez E, Martinerie J, Varela FJ. Measuring phase synchrony in brain signals. Hum Brain Mapp 1999, 8(4).194-208.

33. Mormann F, Lehnertz K, David P, E Elger C. Mean phase coherence as a measure for phase synchronization and its application to the EEG of epilepsy patients. Physica D: Nonlinear Phenomena 2000, 144(3).358-369.

34. Allefeld C, KURTHS J. Multivariate phase synchronization analysis of EEG data. IEICE Transactions on Fundamentals of Electronics, Communications and Computer Sciences 2003, 86(9).2218-2221.

35. Allefeld C, Kurths J. An approach to multivariate phase synchronization analysis and its application to event-related potentials. International Journal of Bifurcation and Chaos 2004, 14(02).417-426.

36. Rosenblum MG, Pikovsky AS, Kurths J. Phase synchronization of chaotic oscillators. Physical Review Letters 1996, 76(11).1804.

37. Li D, Li X, Cui D, Li Z. Phase synchronization with harmonic wavelet transform with application to neuronal populations. Neurocomputing 2011, 74(17).3389-3403.

38. Park H, Kim D-S. Evaluation of the dispersive phase and group velocities using harmonic wavelet transform. NDT & E International 2001, 34(7).457-467.

39. Lachaux J-P, Rodriguez E, Le van Quyen M, Lutz A, Martinerie J, Varela FJ. Studying single-trials of phase synchronous activity in the brain. International Journal of Bifurcation and Chaos 2000, 10(10).2429-2439.

40. Tass P, Rosenblum M, Weule J, Kurths J, Pikovsky A, Volkmann J, Schnitzler A, Freund H-J. Detection of n: m phase locking from noisy data: application to magnetoencephalography. Physical Review Letters 1998, 81(15).3291.

41.   Otnes RK, Enochson L. Digital time series analysis. John Wiley & Sons, Inc.; 1972.

42.   Silverman BW. Density estimation for statistics and data analysis. Volume 26. CRC press; 1986.

43.   Beirlant J, Dudewicz EJ, Györfi L, Van der Meulen EC. Nonparametric entropy estimation: An overview. International Journal of Mathematical and Statistical Sciences 1997, 6.17-40.

44.   Steuer R, Kurths J, Daub CO, Weise J, Selbig J. The mutual information: detecting and evaluating dependencies between variables. Bioinformatics 2002, 18 Suppl 2.S231-240.

45.   Qiu P, Gentles AJ, Plevritis SK. Fast calculation of pairwise mutual information for gene regulatory network reconstruction. Comput Methods Programs Biomed 2009, 94(2).177-180.

46.   Bandt C, Pompe B. Permutation entropy: a natural complexity measure for time series. Phys Rev Lett 2002, 88(17).174102.

47.   Liang Z, Wang Y, Ouyang G, Voss LJ, Sleigh JW, Li X. Permutation auto-mutual information of electroencephalogram in anesthesia. Journal of neural engineering 2013, 10(2).026004.

48.   Quiroga RQ, Arnhold J, Grassberger P. Learning driver-response relationships from synchronization patterns. Physical Review E 2000, 61(5).5142.

49.   Breakspear M, Terry J. Topographic organization of nonlinear interdependence in multichannel human EEG. Neuroimage 2002, 16(3).822-835.

50.   Breakspear M, Terry J. Nonlinear interdependence in neural systems: motivation, theory, and relevance. International Journal of Neuroscience 2002, 112(10).1263-1284.

51.   Quiroga RQ, Kraskov A, Kreuz T, Grassberger P. Performance of different synchronization measures in real data: a case study on electroencephalographic signals. Physical Review E 2002, 65(4).041903.

52.   Arnhold J, Grassberger P, Lehnertz K, Elger C. A robust method for detecting interdependences: application to intracranially recorded EEG. Physica D: Nonlinear Phenomena 1999, 134(4).419-430.

53.   Eckmann J-P, Kamphorst SO, Ruelle D. Recurrence plots of dynamical systems. Europhys Lett 1987, 4(9).973-977.

54.   Zbilut JP, Giuliani A, Webber CL. Detecting deterministic signals in exceptionally noisy environments using cross-recurrence quantification. Physics Letters A 1998, 246(1).122-128.

55.   Marwan N, Kurths J. Nonlinear analysis of bivariate data with cross recurrence plots. Physics Letters A 2002, 302(5).299-307.

56.   Webber Jr CL, Zbilut JP. Dynamical assessment of physiological systems and states using recurrence plot strategies. Journal of Applied Physiology 1994, 76(2).965-973.

57.   Zbilut JP, Webber Jr CL. Embeddings and delays as derived from quantification of recurrence plots. Physics Letters A 1992, 171(3).199-203.

58.   Smith WD, Dutton RC, Smith NT. Measuring the performance of anesthetic depth indicators. Anesthesiology 1996, 84(1).38-51.

59.   Shalbaf R, Behnam H, Sleigh J, Voss L. Using the Hilbert–Huang transform to measure the electroencephalographic effect of propofol. Physiological Measurement 2012, 33(2).271.

60.   Williams M, Sleigh J. Auditory recall and response to command during recovery from propofol anaesthesia. Anaesthesia and intensive care 1999, 27(3).265.

61.   Li X, Li D, Liang Z, Voss L, Sleigh J. Analysis of depth of anesthesia with Hilbert-Huang spectral entropy. Clinical Neurophysiology 2008, 119(11).2465-2475.

62.   Delorme A, Makeig S. EEGLAB: an open source toolbox for analysis of single-trial EEG dynamics including independent component analysis. Journal of neuroscience methods 2004, 134(1).9-21.

63.   Seo S. A review and comparison of methods for detecting outliers in univariate data sets. University of Pittsburgh; 2006.

64.   Fatourechi M, Bashashati A, Ward RK, Birch GE. EMG and EOG artifacts in brain computer interface systems: A survey. Clinical Neurophysiology 2007, 118(3).480-494.

65.   Schlögl A. The electroencephalogram and the adaptive autoregressive model: theory and applications. Shaker Germany; 2000.

66.   Cimenser A, Purdon PL, Pierce ET, Walsh JL, Salazar-Gomez AF, Harrell PG, Tavares-Stoeckel C, Habeeb K, Brown EN. Tracking brain states under general anesthesia by using global coherence analysis. Proc Natl Acad Sci U S A 2011, 108(21).8832-8837.

67.   Sleigh JW, Donovan J. Comparison of bispectral index, 95% spectral edge frequency and approximate entropy of the EEG, with changes in heart rate variability during induction of general anaesthesia. Br J Anaesth 1999, 82(5).666-671.

68.   Vakkuri A, Yli-Hankala A, Talja P, Mustola S, Tolvanen-Laakso H, Sampson T, Viertio-Oja H. Time-frequency balanced spectral entropy as a measure of anesthetic drug effect in central nervous system during sevoflurane, propofol, and thiopental anesthesia. Acta Anaesthesiol Scand 2004, 48(2).145-153.

69.   Schrouff J, Perlbarg V, Boly M, Marrelec G, Boveroux P, Vanhaudenhuyse A, Bruno MA, Laureys S, Phillips C, Pelegrini-Issac M, Maquet P, Benali H. Brain functional integration decreases during propofol-induced loss of consciousness. Neuroimage 2011, 57(1).198-205.

Appendix A

In order to evaluate the synchronization changes in different anesthetic states efficiently, we discussed the parameter selections of PS, NI and DET. We calculated these synchronization indexes under different parameters of all subjects and chose three datasets from each synchronization index in awake, unconscious and recovery states which were according to the time points of each subjects. The values of synchronization indexes under different parameters were shown in Fig. S1-S4. All values were given by median (Q1, Q3).

1. PS

Fig. S1 and Fig. S2 showed the PS_{PLV} (δ, θ, α, β and $\gamma1$) and PS_{SE} (δ, θ, α, β and $\gamma1$) values at different epoch length T_e in awake state (red), unconscious state (green) and recovery state (blue) of all subjects. It can be seen from Fig. S1 that the PS_{PLV} values of all frequency bands decreased with increasing T_e. The difference between awake and unconscious states of PS_{PLV} (δ) were larger than PS_{PLV} in other frequency bands, which was also could be seen from Fig. 4F. By contrast, PS_{SE} had some fluctuation at different T_e (Fig. S2). T_e =20 was used in our study.

<div align="center">"Fig. S1"</div>

<div align="center">"Fig. S2"</div>

2. NI

Fig. S3A showed the NI values with time lag τ=1, nearest neighbors k=20 in different embedding dimension m in awake state (red), unconscious state (green) and recovery state (blue) of all subjects. The NI values with τ=2, k=20 in different m were shown in Fig. S3B. As can be seen from these two figures, NI increased monotonically with increasing m and the difference of NI values between awake, unconscious and recovery states became wider with increasing m. Therefore, m=5 was selected in terms of calculation complexity. Fig. S3C showed NI values with m=5, k=20 in different τ. The NI difference between awake and unconscious states became smaller with increasing τ, so we chose τ=1. The NI values with m=5, τ=1 in different nearest neighbors k were shown in Fig. S3D and we selected k=20.

<div align="center">"Fig. S3"</div>

3. DET

Fig. S4A, Fig. S4B and Fig. S4C showed DET values with embedding dimension $m=3$, $m=4$ and $m=5$ respectively in threshold of diagonal length $l_{min}=2$ in different time lag τ in awake state (red), unconscious state (green) and recovery state (blue) of all subjects. $m=3$, $\tau=2$ were selected because of the great DET difference between awake and unconscious states. DET values with $m=3$, $\tau=2$ in different l_{min} were shown in Fig. S4D and $l_{min}=2$ was selected.

"Fig. S4"

Appendix B

We used the MATLAB programs *lagged.m* to compute COR, which can be downloaded from the Functional Connectivity Toolbox (https://sites.google.com/site/functionalconnectivity toolbox/). The MATLAB programs of PS_{SE} and PS_{CP} (*nbt_n_m_detection.m*) can be downloaded from the Neurophysiological Biomarker Toolbox (https://www.nbtwiki.net/doku.php?id=tutorial:phase_locking_ value#.VWm2zmgyGlB). The MATLAB programs of KerMI (*FastPairMI.m*) can be downloaded from http://pengqiu.gatech.edu/software/FastPairMI/index.htm. The MATLAB program of NI (*synchro.m*) can be downloaded from https://vis.caltech.edu/~rodri/software.htm. The MATLAB programs of PCMI, PS_{PLV}, DET and WTC are available by contacting the corresponding author.
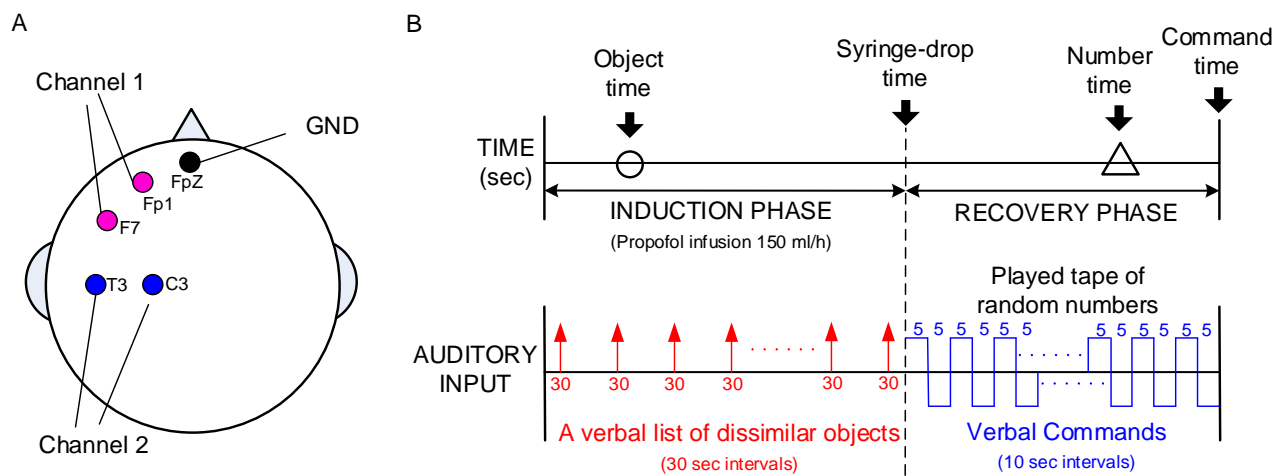
Figures

Fig. 1 (A) Positions of scalp electrodes at Fp1-F7 and C3-T3. (B) The diagram of experimental sequence. The "Object time" (circle),"Syringe-drop time", "Number time" (triangle) and "Command time" were marked in the diagram. A verbal list of dissimilar objects was executed in 30-second intervals in the induction phase. The tape of random numbers was played and verbal commands were given in 10-second intervals in the recovery phase.
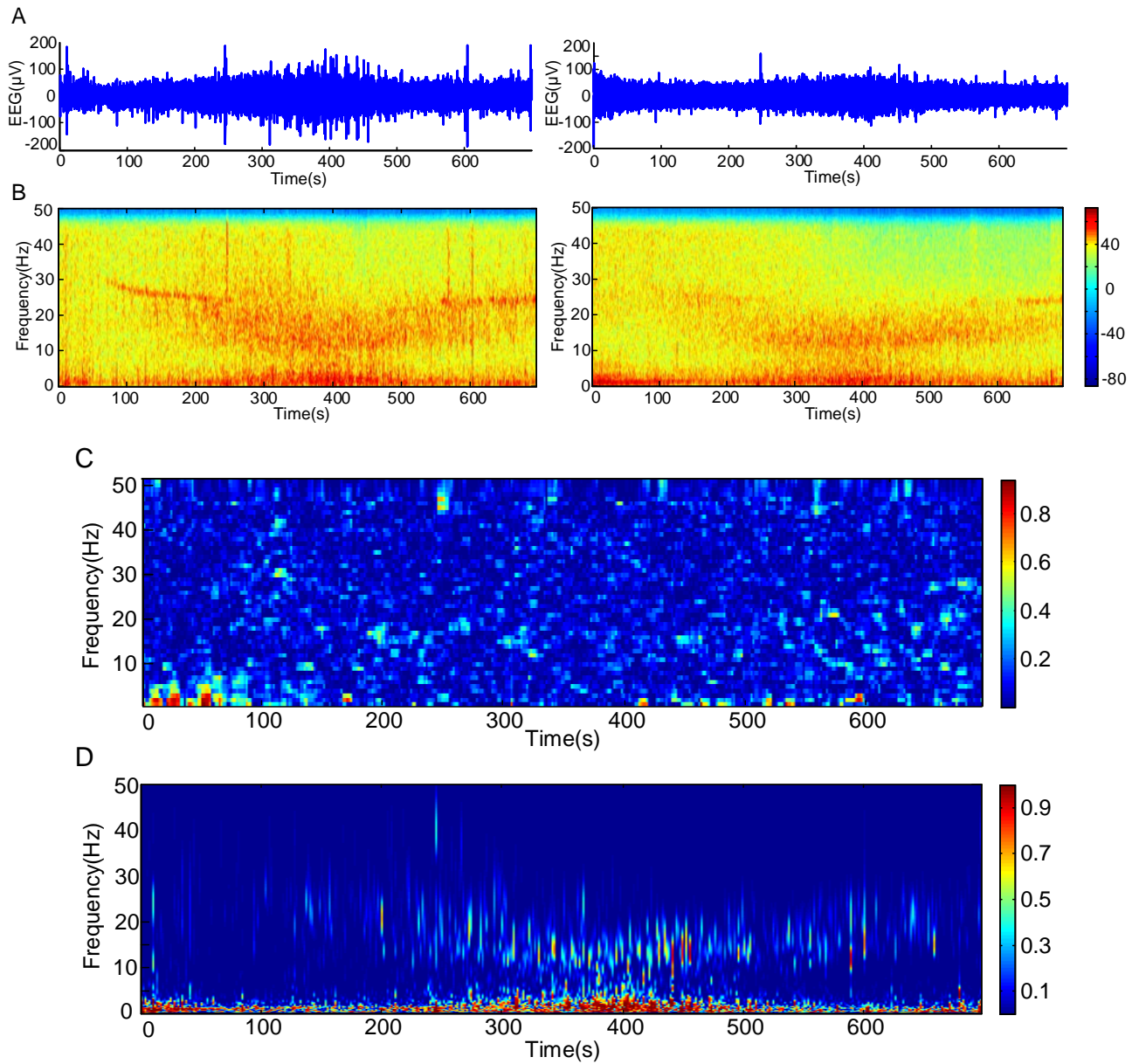
Fig. 2 (A) Two-channel preprocessed EEG recordings of one subject over the whole experiment period. (B) The spectrograms of the EEG recordings computed by a short-time Fourier transform. (C) The FTC spectrum of the two EEG recordings. (D) The WTC spectrum of the two EEG recordings.
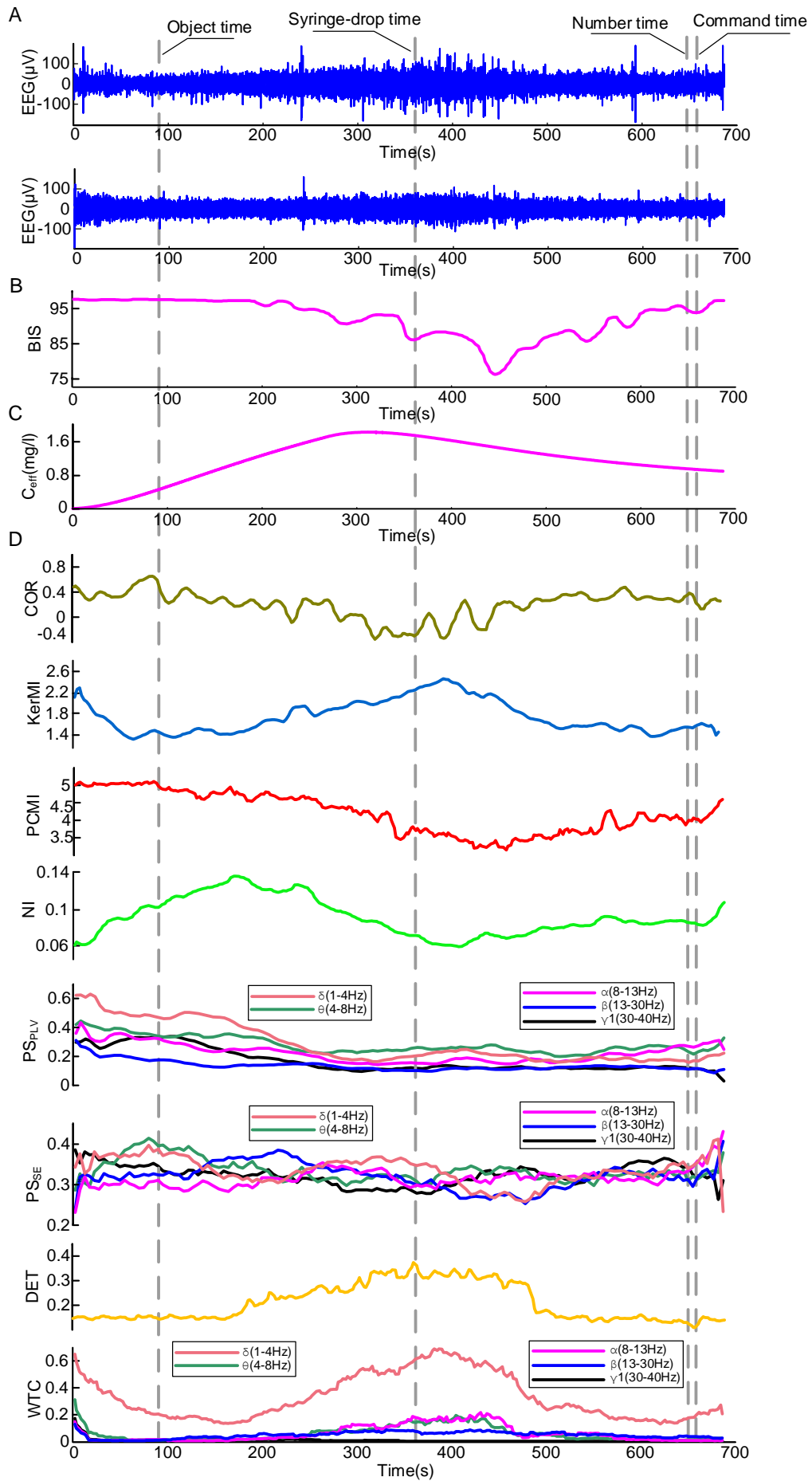
Fig. 3 (A) Two-channel preprocessed EEG recordings of one subject over the whole experiment period. (B) BIS value of the same subject. (C) C_{eff} value of the same subject. (D)The synchronization index values of the same subject. Four dashed gray lines denoted the four time points in the experiment.
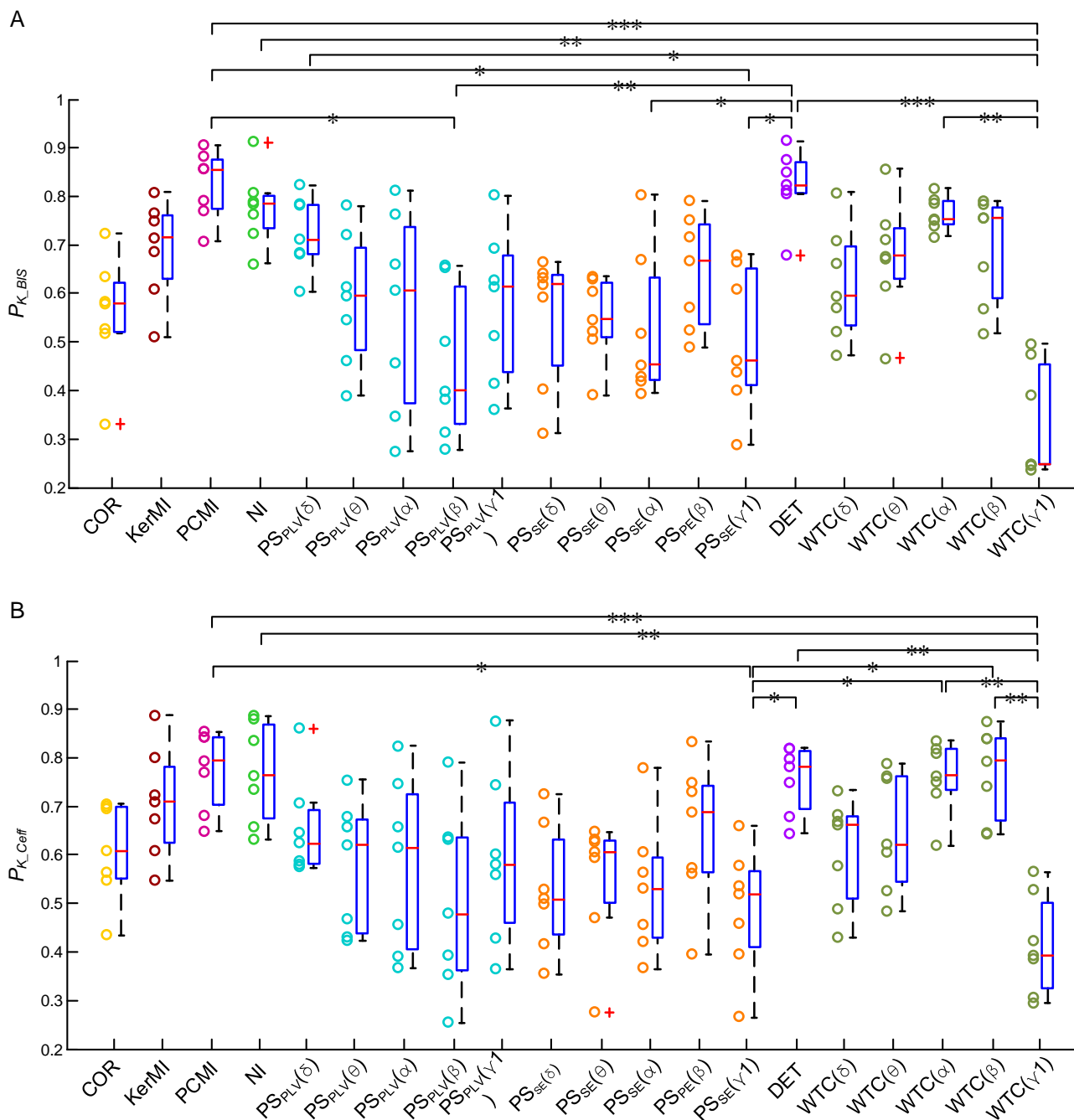

Fig. 4 (A) Prediction probability P_K values of synchronization indexes with BIS of all subjects. (B) The P_K values of synchronization indexes with C_{eff} of all subjects. The notation *, ** and *** indicate significant difference at $p<0.05$, $p<0.01$ and $p<0.001$ respectively, through Friedman test and Multiple comparison test.

Fig. 5 Box plots of synchronization indexes in different studied periods (I: awake state, II: unconscious state, III: recovery state). The notation *, ** and *** indicate significant difference at $p<0.05$, $p<0.01$ and $p<0.001$ respectively, through Kruskal-Wallis test and Multiple comparison test.
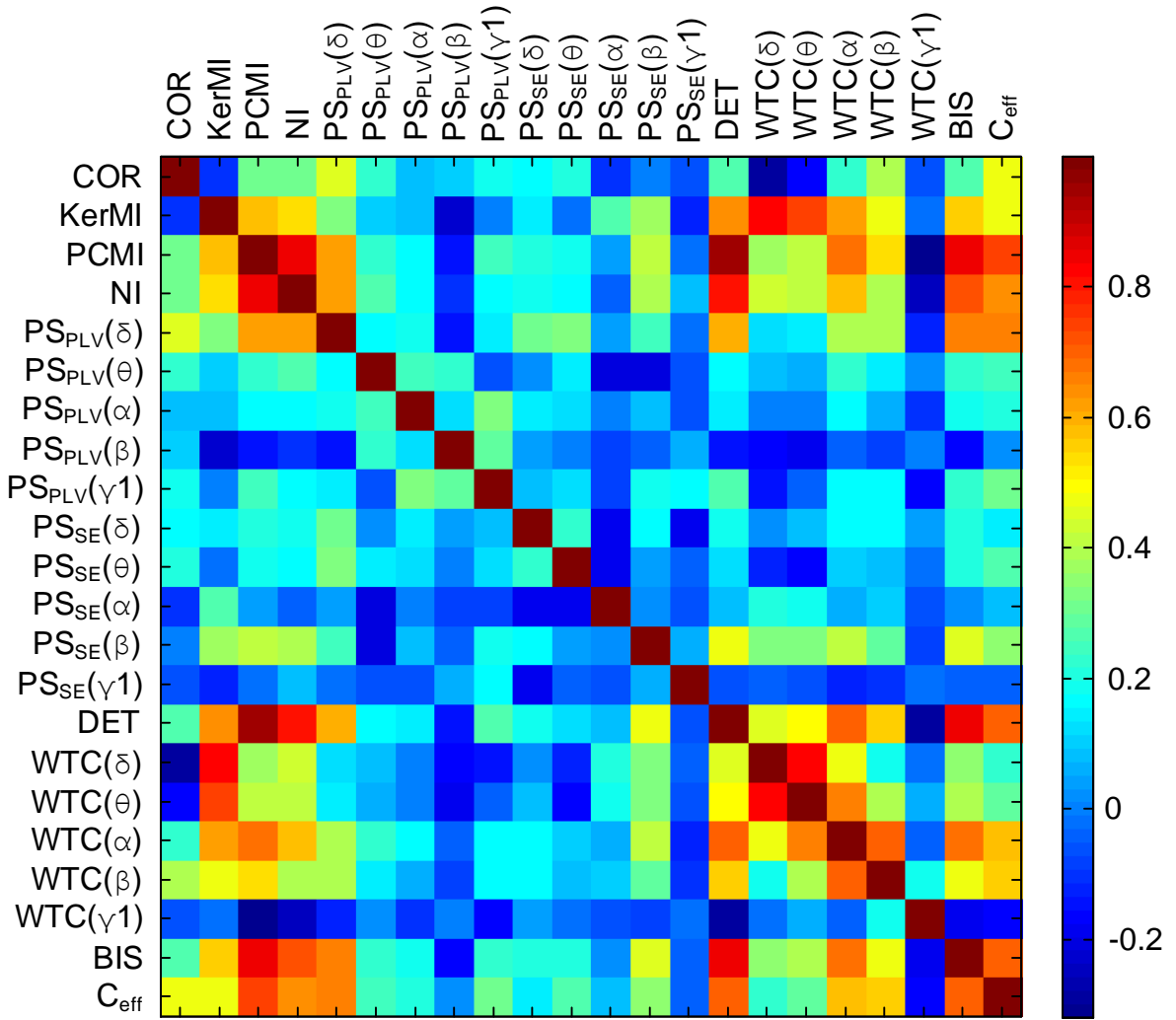
Fig. 6 Correlation coefficient R among synchronization indexes, BIS and C_{eff} averaged over all subjects.

Tables

Table 1 The event times for each subject

Subject	"Object time" (s)	"Syringe-drop time"(s)	"Number time" (s)	"Command time" (s)
#1	180	283	435	475
#2	90	357	639	649
#3	90	421	792	802
#4	30	454	*	650
#5	90	202	*	545
#6	30	401	822	832
#7	90	355	560	570

"Object time" = the time point of the last object remembered for the subject during the induction phase.

"Syringe-drop time" = the time point that the subject dropped the syringe, denoting the end the induction and loss of consciousness.

"Number time" = the time point of the first number remembered during recovery.

* Subjects who did not remember any number until responding to verbal command.

"Command time" = the time point corresponding to the subject's correct response to verbal command.

Table 2 Median, Q1 and Q3 of P_K of different synchronization indexes with BIS and C_{eff}

		COR	KerMI	PCMI	NI	$PS_{PLV}(\delta)$	$PS_{PLV}(\theta)$	$PS_{PLV}(\alpha)$	$PS_{PLV}(\beta)$	$PS_{PLV}(\gamma 1)$	$PS_{SE}(\delta)$
	median	0.579	0.714	0.855	0.783	0.711	0.595	0.605	0.399	0.613	0.619
BIS	Q1	0.519	0.629	0.775	0.734	0.681	0.482	0.373	0.331	0.438	0.450
	Q3	0.621	0.760	0.875	0.802	0.783	0.694	0.737	0.614	0.677	0.639
	median	0.607	0.709	0.794	0.764	0.624	0.621	0.615	0.479	0.580	0.509
C_{eff}	Q1	0.552	0.625	0.703	0.676	0.582	0.440	0.408	0.363	0.460	0.437
	Q3	0.699	0.781	0.842	0.868	0.692	0.672	0.725	0.636	0.708	0.633
		$PS_{SE}(\theta)$	$PS_{SE}(\alpha)$	$PS_{SE}(\beta)$	$PS_{SE}(\gamma 1)$	DET	WTC(δ)	WTC(θ)	WTC(α)	WTC(β)	WTC$(\gamma 1)$
	median	0.545	0.453	0.667	0.460	0.823	0.594	0.677	0.753	0.755	0.248
BIS	Q1	0.510	0.420	0.536	0.409	0.806	0.534	0.628	0.742	0.590	0.246
	Q3	0.622	0.632	0.743	0.650	0.869	0.697	0.734	0.790	0.777	0.453
	median	0.605	0.530	0.688	0.520	0.781	0.662	0.621	0.763	0.794	0.393
C_{eff}	Q1	0.502	0.430	0.561	0.411	0.695	0.511	0.546	0.733	0.670	0.327
	Q3	0.630	0.595	0.743	0.568	0.816	0.679	0.762	0.817	0.840	0.503

COR = cross correlation;

KerMI = mutual information based on kernel estimation;

PCMI = permutation cross mutual information;

NI = nonlinear interdependence;

PS_{PLV} = phase synchronization based on phase locking value;

PS_{SE} = phase synchronization based on Shannon entropy;

DET = determinism;

WTC = coherence based on wavelet transformation;

Table 3 CV (SD/mean) of the studied indexes at different anesthetic states

	Awake	Unconscious	Recovery
COR	$0.1933/0.3056 \approx 0.633$	$0.0711/0.3819 \approx 0.186$	$0.1309/0.4375 \approx 0.299$
KerMI	$0.1661/0.2654 \approx 0.627$	$0.1547/0.6831 \approx 0.227$	$0.2229/0.4071 \approx 0.548$
PCMI	$0.3910/4.5818 \approx 0.085$	$0.4223/2.9029 \approx 0.146$	$0.4286/4.0663 \approx 0.105$
NI	$0.0271/0.1231 \approx 0.220$	$0.0105/0.0634 \approx 0.165$	$0.0203/0.0971 \approx 0.209$
$PS_{PLV}(\delta)$	$0.0835/0.3444 \approx 0.243$	$0.0527/0.1881 \approx 0.280$	$0.0666/0.2065 \approx 0.323$
$PS_{PLV}(\theta)$	$0.0490/0.2684 \approx 0.183$	$0.0560/0.2133 \approx 0.263$	$0.0612/0.2334 \approx 0.262$
$PS_{PLV}(\alpha)$	$0.0857/0.2448 \approx 0.350$	$0.0552/0.1905 \approx 0.290$	$0.0682/0.2210 \approx 0.309$
$PS_{PLV}(\beta)$	$0.0369/0.1131 \approx 0.326$	$0.0627/0.1279 \approx 0.490$	$0.0584/0.1217 \approx 0.480$
$PS_{PLV}(\gamma1)$	$0.0735/0.1495 \approx 0.491$	$0.0258/0.1011 \approx 0.255$	$0.0438/0.1025 \approx 0.427$
$PS_{SE}(\delta)$	$0.0326/0.3436 \approx 0.095$	$0.0477/0.3378 \approx 0.141$	$0.0620/0.3356 \approx 0.185$
$PS_{SE}(\theta)$	$0.0230/0.3598 \approx 0.064$	$0.0206/0.3475 \approx 0.059$	$0.0548/0.3098 \approx 0.177$
$PS_{SE}(\alpha)$	$0.0622/0.3453 \approx 0.180$	$0.0125/0.3260 \approx 0.038$	$0.0521/0.3362 \approx 0.155$
$PS_{SE}(\beta)$	$0.0322/0.3604 \approx 0.089$	$0.0250/0.3173 \approx 0.079$	$0.0348/0.3623 \approx 0.096$
$PS_{SE}(\gamma1)$	$0.0256/0.3116 \approx 0.082$	$0.0181/0.3133 \approx 0.058$	$0.0324/0.3139 \approx 0.103$
DET	$0.0398/0.1758 \approx 0.226$	$0.0503/0.3651 \approx 0.138$	$0.0570/0.2115 \approx 0.269$
$WTC(\delta)$	$0.1119/0.1637 \approx 0.684$	$0.1568/0.3272 \approx 0.479$	$0.0958/0.1506 \approx 0.636$
$WTC(\theta)$	$0.0211/0.0175 \approx 1.206$	$0.0617/0.0830 \approx 0.743$	$0.0128/0.0131 \approx 0.981$
$WTC(\alpha)$	$0.0146/0.0109 \approx 1.334$	$0.0751/0.1065 \approx 0.705$	$0.0230/0.0206 \approx 1.118$
$WTC(\beta)$	$0.0063/0.0039 \approx 1.595$	$0.0437/0.0595 \approx 0.733$	$0.0228/0.0278 \approx 0.822$
$WTC(\gamma1)$	$0.0080/0.0028 \approx 2.89$	$0.0009/0.0007 \approx 1.356$	$0.0317/0.0153 \approx 2.077$

The meaning of the indexes refers to the legend of Table 2